Normal mode analysis of mouse epidermal growth factor: Characterization of the harmonic motion

ARTICLE *in* PROTEINS STRUCTURE FUNCTION AND BIOINFORMATICS · AUGUST 1993

Impact Factor: 2.63 · DOI: 10.1002/prot.340160410

2 AUTHORS, INCLUDING:

Nobuhiro Go
Japan Atomic Energy Agency
238 PUBLICATIONS **9,743** CITATIONS

SEE PROFILE

PROTEINS: Structure, Function, and Genetics 16:423–436 (1993)

Normal Mode Analysis of Mouse Epidermal Growth Factor: Characterization of the Harmonic Motion

Teikichi Ikura and Nobuhiro Gō
Department of Chemistry, Faculty of Science, Kyoto University, Kyoto 606, Japan

ABSTRACT **Normal mode analysis of mouse epidermal growth factor (mEGF) has been carried out at room temperature. The value of the lowest frequency is 4.1 cm^{-1}. This mode corresponds to hinge-bending motion between the N-terminal and C-terminal domains of mEGF. This hinge-bending motion corresponds to the "mitten mode." In this motion, the N-terminal domain is almost rigid. However, the C-terminal domain is found to consist of three rigid segments. Two segments, C33-D46 and G51-R53, are observed moving in the same direction, but L47-W50 moves in the opposite direction. For this mode, the effective Young's modulus turned out to be 1.1 × 10^9 dyn·cm^{-2}. This value is a little larger than that of the mode with the lowest frequency 4.4 cm^{-1} of BPTI. The difference may be related to the fraction of residues involved in β-sheets in the molecule. Similar analyses are carried out for other low frequency modes.** © 1993 Wiley-Liss, Inc.

Key words: conformational dynamics, mitten model, hinge bending motion, Young's modulus, low frequency mode

INTRODUCTION

Epidermal growth factor (EGF) is a small single-chain protein containing 53 amino acids and three disulfide bonds, first isolated by Cohen from mouse submaxillary glands.[1–3] EGF stimulates growth and differentiation of various epidermal and epithelial tissues, and human EGF (hEGF) may function physiologically to inhibit gastric acid secretion. EGF and EGF-like proteins may also play a role in oncogenesis and wound healing.[4–6]

In recent years, there have been many structural studies on EGF by using NMR experiments. Three-dimensional structures of mouse EGF (mEGF) were determined independently by two research groups, Kohda et al.[7,8] and Montelione et al.[9–11] The structures determined by the two groups were very similar to each other. Mouse EGF consists of the N-terminal domain (N1-N32) and the C-terminal domain (C33-R53) (refer to Fig. 1). In the N-terminal domain, there is an antiparallel β-sheet structure (V19-I23 and S28-N32). Such a β-sheet structure has also been reported for human des(49-53-)-EGF and intact human EGF. The segment, N1-P4, is loosely attached to the β-sheet structure in an antiparallel manner. The successive segment, G5-C14, takes a right-handed helix-like structure and the segment, L15-V19, forms a turn structure. The sidechains of P7, Y10, Y13, H22, and Y29 form a hydrophobic core in the N-terminal domain. In the C-terminal domain, the segment, C33-D46, adopts a "double hairpin" structure, with a type II β-turn at I35-G36 and a loop structure in the segment, G39-Q43. The sidechains of V34, I35, Y37, W49, and W50 form a hydrophobic core in the C-terminal domain. The segment, L47-R53, is located at the periphery of the C-terminal core. The shape of mEGF is well characterized by a mitten model. The mitten is right-handed, and consists of a palm (N-terminal domain) and a thumb (C-terminal domain). In the mitten model, it is implied that the hollow between the two domains may function as a binding site for the EGF receptor.

Comparing the structures of mEGF determined by the two groups, the relative orientations of the two domains were found to be slightly different. In Kohda et al.'s model[8], the C-terminal domain was placed closer to the N-terminal domain than in Montelione's.[10] This difference appears to be caused by the number of interdomain NOEs. Only a few interdomain NOEs were observed by both groups. This limited number of NOEs allowed some varieties of orientations of the two domains. Recently, Montelione et al.[12] reported a more refined structure obtained by energy minimization with a more number of newly measured NOE restraints. The gross structure is the same as that described previously. However, in the absence of atomic coordinates, it is not possible to compare these structures in detail.

Recently, many attempts have been made to determine those amino acid residues of EGF and the related transforming growth factor (TGFα) that are directly involved in intermolecular interactions with the EGF receptor. For hEGF, the results of receptor-binding experiments, using monoclonal anti-

Received November 17, 1992; accepted March 1, 1993.
Address reprint requests to Dr. Nobuhiro Gō, Department of Chemistry, Faculty of Science, Kyoto University, Sakyo-ku, Kyoto 606, Japan.

bodies and monospecific polyclonal antibodies, suggested that the segment, H22-N32, was involved in the receptor binding, but that the segments, N1-W13 and W13-C20, were not directly involved.[13] Several analogues of hEGF having specific amino acid substitutions in the β-sheet structure of the N-terminal domain indicated that hydrophobic amino residues (V19, M21, I23, L26) on the exposed surface of the β-sheet structure have an important role in the formation of the active EGF-receptor complex.[14] The studies using the enzymatic digestion of C-terminus of mEGF indicated that L47 is intimately involved in the formation of the ligand-receptor complex.[15] The experimental technique of site-directed mutagenesis is giving us more information on the receptor-binding of EGF, in addition to the above experimental data. These experimental results were helpful to understand the function of EGF.

In general, a protein molecule performs its biological function by binding to its ligand or receptor. Shape of a protein is important in this binding. This relation between a protein and a ligand or receptor is expressed by the "lock and key" concept. However, evidence is accumulating which indicates that protein structures behave dynamically in the course of binding. Therefore, it is necessary to understand also the dynamics of a protein molecule in order to elucidate its function at the molecular structural level.

In the present study, we carry out the normal mode analysis of mEGF. The mitten model described by Kohda et al.[8] suggests existence and biological importance of the opening and closing of the mitten. Our main interest focuses on the motion suggested by the mitten model.

We will follow mostly the method of analysis developed by Nishikawa and Gō[16] for studying the dynamic structure of bovine pancreatic trypsin inhibitor (BPTI). This method of analysis has also been applied by Gibrat and Gō[17] to human lysozyme. The results of the analysis for mEGF will be compared with those obtained previously for BPTI and human lysozyme to learn about features common to globular proteins and specific to each specific protein.

MATERIALS AND METHODS

Minimum Energy Conformation

A minimum energy conformation (MEC) of mEGF is obtained by minimizing its conformational energy function

$$f = \alpha F_1 + F_2$$

where F_1 is the DADAS[18,19] penalty function corresponding to NOEs, F_2 is the ECEPP[20] energy function, and α is a weighting factor. By starting with a large value of α and gradually decreasing α (finally $\alpha = 0$), it should be possible at some stage to obtain a structure in which the majority of NMR constraints are still satisfied, while at the same time all of the interatomic electrostatic and nonbonded interactions are energetically favorable.

TABLE I. Summary of Residual Violations of Constraints in the DGC

No. of upper bound constraint violations			No. of steric violations	
0.1–0.3 Å	0.3 Å<	Max. value (Å)	0.1 Å<	Max. value (Å)
14	3	0.40	1	0.10

Normal Mode Analysis

The normal mode analysis is done by following the method described previously.[16] We calculate the second derivative matrix (the hessian) at the minimum point and the coefficient matrix for the kinetic energy when this latter is expressed as a function of the generalized coordinates. Next, we solve the generalized eigenvalue problem. The eigenvalues give the vibrational time scales (frequencies) and the eigenvectors give the principal axes of the quadratic. These axes are the directions in the variable space where the value of the quadratic is expressed as a sum of squares without any cross-terms and are therefore independent of each other.

RESULTS

Minimum Energy Conformation

We obtained a minimum energy conformation of mEGF by starting from the best distance geometry conformation (DGC), which satisfied most of the distance constraints (Table I) and by decreasing the weighting factor α very gradually. However, in the obtained MEC, several distance constraints corresponding to NOEs were observed to be violated. Values of residual violation of 8 upper distance constraints were more than 1.0 Å (Table II). These violated constraints were mainly those connecting the two domains. Furthermore, the large conformational change was observed during the energy minimization at residues V34-Y37. A hydrogen bond, V34(H^N) . . . Y37(O), was broken. Because these violations were mainly observed at constraints connecting the two domains, we investigated the contact between the two domains in both DGC and MEC. In the DGC, a turn structure L15-V19 of the N-terminal domain is located closer to a loop structure G39-Q43 of the C-terminal than in the MEC. The change of the arrangement of these two segments may cause the deformation of V34-Y37. These rather large conformational changes during the energy minimization appear to be caused by the absence of hydrogen bonds involving solvent water and also by artificially emphasized electrostatic interac-

TABLE II. List of Upper Bound Distance Constraints of Which Values of Residual Violation Are More Than 1.0 Å in the MEC

$Y3(H^N)$–$M21(H^\beta)$	$L15(H^\delta)$–$R41(H^\gamma)$
$P4(H^\delta)$–$M21(H^\beta)$	$L15(H^\delta)$–R41(NH)
$P7(H^\delta)$–$H22(H^{\epsilon 1})$	$L15(H^\delta)$–$Q43(H^\alpha)$
$Y13(H^{3,5})$–$R41(H^\beta)$	$H22(H^{\epsilon 1})$–$D27(H^\alpha)$

tions in vacuum. Figure 1 shows the stereoview of the superposition of the DGC and the MEC. The root-mean-square (rms) displacement is calculated. The backbone rms displacement was 1.9, 1.1, 1.0 Å in the whole molecule, N1-V34, and S38-W49, respectively.

Frequency Histogram

Distribution of the calculated frequencies is shown in the histogram of Figure 2a. Because the number of independent variables in our present treatment is 297, we obtained this number of normal modes and frequencies. The lowest and highest frequencies are 4.1 cm^{-1} and 948.6 cm^{-1}, respectively. The modes with frequencies below 30, 120, 200, 300 cm^{-1} account for 12.8, 57.9, 75.8, and 85.9% of all modes, respectively. The distribution obtained here for mEGF is very similar to that obtained previously for a number of globular proteins.[16]

Each mode contributes to the mass-weighted mean-square fluctuation of atomic positions by a quantity given by $kT/(2\pi\nu)^2$. Normal modes with very low frequencies have dominant contributions. Figure 2b shows cumulative contribution from modes with the frequency indicated on the abscissa or lower.

Site Dependence of Fluctuations of Dihedral Angles

Rms thermal fluctuations for ω, ϕ, and ψ are plotted against residue number in Figure 3a. The amplitudes of fluctuations of ω are rather uniform over residues, and its mean value is 5.68°. Those of ϕ and ψ differ considerably from site to site. Their mean values are 7.46° and 8.55°, respectively. The values are observed to be small in the neighborhoods of Y10, L26, R41, D46, and L52. Except L52, these are located in the turn region or in the loop region. In Figure 3b, peak frequency of backbone dihedral angles, i.e., the frequency of the normal mode with the largest contribution to the mean-square fluctuation of the backbone dihedral angles of a residue, is plotted against residue number. The peak frequency ranges from 5.2 cm^{-1} to 274.4 cm^{-1}. By comparing Figure 3a and 3b, we see that regions of small fluctuations have high peak frequencies, which are more than about 150 cm^{-1}. On the contrary, regions of large fluctuations (S2, G5, G18, V19, S28, and Y29) have low peak frequencies (the mean value is less than 15 cm^{-1}). These results indicate that site dependence of fluctuations of protein backbone are mainly determined by modes with very low frequencies.

Fluctuations of C^α Atoms

Figure 4a shows the rms fluctuations of C^α atoms calculated by the normal mode analysis as the square root of a sum of contributions from all modes. The smallest and largest values of rms fluctuations are 0.33 Å at Y29 and 0.86 Å at L26, respectively. The mean value is 0.48 Å. L26 is located at the turn of the β-sheet of the N-terminal domain. Y29 is located at the β-sheet. Another residue, M21, with a small value of r.m.s. fluctuation is also located at the β-sheet. Figure 4b shows the rms fluctuations of C^α atoms as the square root of sums of contributions from all modes with frequencies below and above a border frequency 30 cm^{-1}, respectively. We can understand that modes with frequencies less than 30 cm^{-1}, make major contributions to the thermal fluctuations. We also see that the contributions from modes with frequencies above 30 cm^{-1} do not have clear site dependence. If we take a frequency lower than 30 cm^{-1} as the border frequency, then site dependence begins to be observed also in the contributions from modes with frequencies above the border value. Therefore, the site dependence of rms fluctuations of C^α atoms is determined mainly by modes with frequencies below 30 cm^{-1}. Modes with frequencies above 30 cm^{-1} contribute mainly to site-independent "background" motions. Similar results were observed in the analyses of dynamics of BPTI.[16]

Localization of Atomic Displacement Vectors in Each Mode

Radius of localization of atomic displacement vectors in each normal mode[16] are calculated, and are shown in Figure 5. Stereo drawings of atomic displacement vectors in three modes with high, medium, and low frequencies are shown in Figure 6. From these figures we see the following.

In 172 modes with frequencies lower than 120 cm^{-1}, the radii of localization are mostly in the range of 10–15 Å and the sites of localization are centered in the middle of the molecule. These values of radii indicate that the whole molecule is involved in the motion of each mode. Stereo drawing of atomic displacement vectors in a mode with frequency of 30.8 cm^{-1} is shown in Figure 6a. The radius of localization in this mode is 12.9 Å.

In 83 modes with frequencies between 120 cm^{-1} and 300 cm^{-1}, the radii of localization are 3–12 Å, and the sites of localization are located within one or two residues from the surface of the molecule. The above values of the radii of localization indicate that the extent of atomic movements ranges from those involving a few residues to those involving the whole molecule. Stereo drawing of atomic displace-

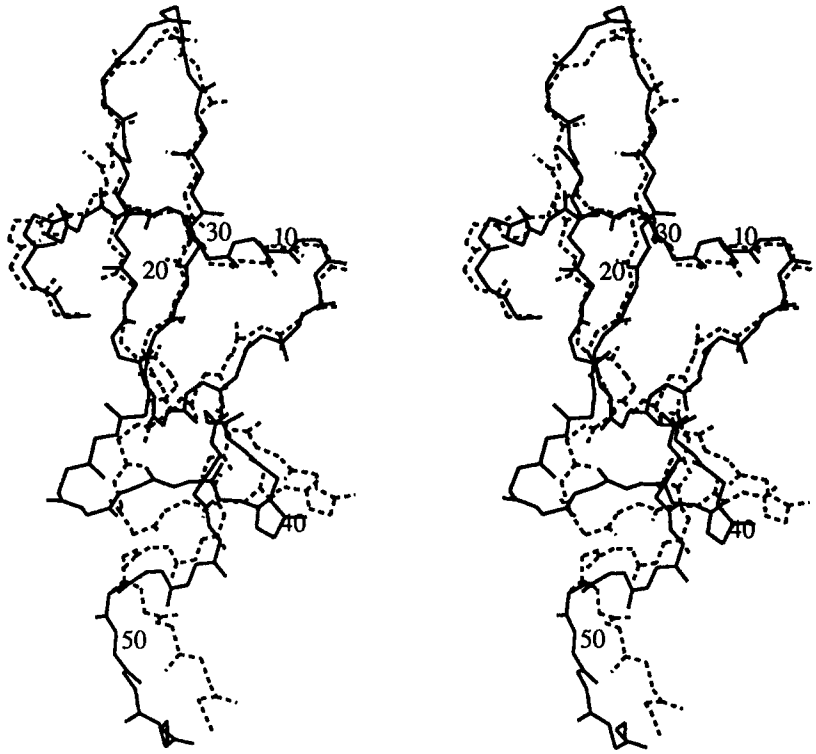

Fig. 1. Stereoview showing the superposition of the polypeptide backbones of the DGC (solid line) and the MEC (broken line). The N, C^{α}, C′ and O atoms are shown.

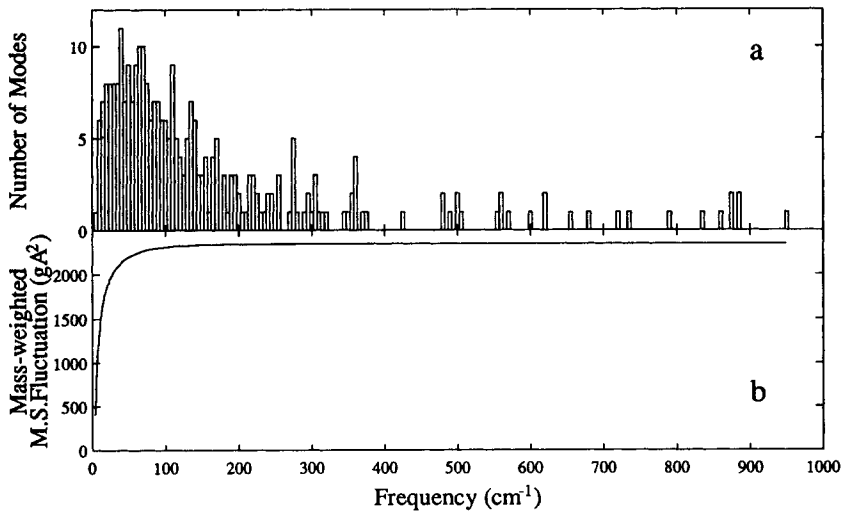

Fig. 2. **a:** Frequency distribution. Number of modes in each interval of 5 cm^{-1}. **b:** Cumulative contribution to the mass-weighted mean-square fluctuation of atomic position from modes with the frequency indicated on the abscissa or lower.

ment vectors in a mode with frequency of 150.7 cm^{-1} is shown in Figure 6b. The radius of localization is 10.5 Å.

In 42 modes with frequencies higher than 300 cm^{-1}, the radii of localization are 2–6 Å, and the sites of localization are located at ends of surface-exposed sidechains. The above values of the radii of localization indicate that only a few atoms at the ends of sidechains are involved in these modes. Stereo drawing of atomic displacement vectors in a mode with frequency of 350 cm^{-1} is shown in Figure 6c. The radius of localization is 3.0 Å.

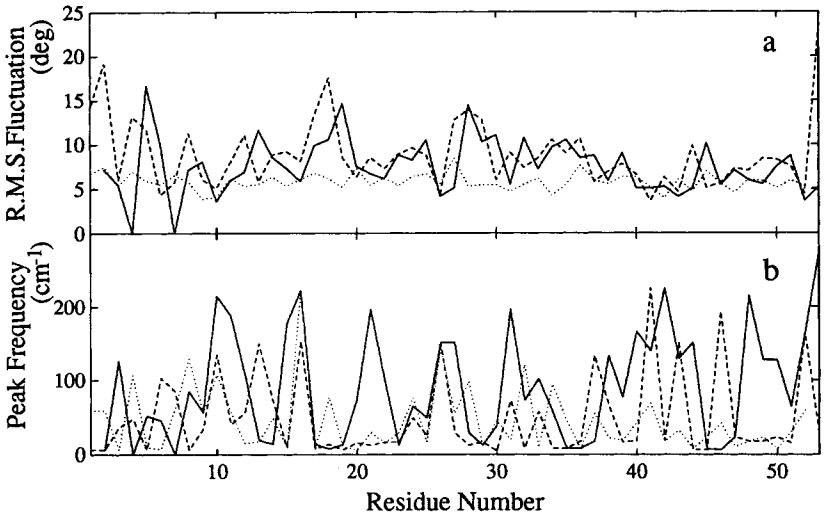

Fig. 3. Site dependence of fluctuations of dihedral angles. **a:** Root-mean-square thermal fluctuations of dihedral angles ω, ϕ and ψ are plotted against residue number. **b:** Peak frequency in the fluctuations of the dihedral angles are plotted against residue number. Solid line, ϕ; broken line, ψ; dotted line, ω. Because the ϕ of P4 and P7 are constant at 75.0°, the rms fluctuations of these angles are zero.

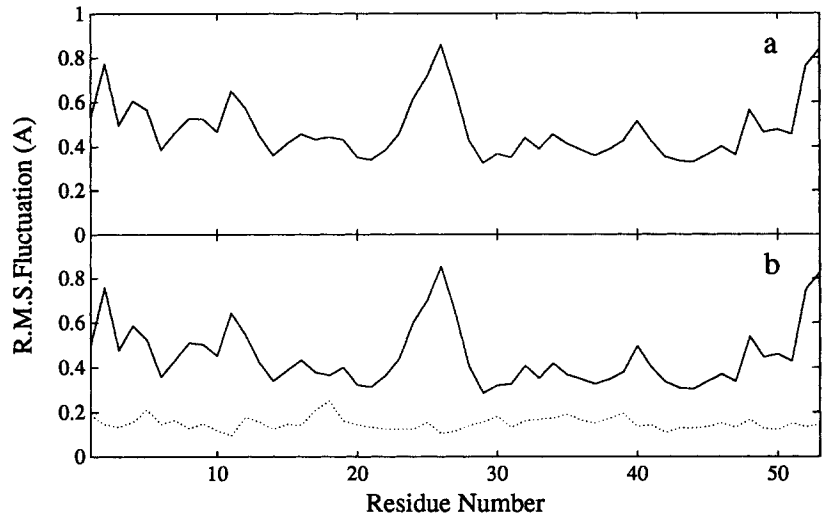

Fig. 4. Site dependence of fluctuations of positions of C^{α} atoms, as square root of a sum of contributions from all modes **(a)**, from modes with frequencies less (solid line) and larger (dotted line) than 30 cm^{-1} **(b)**, plotted against residue number.

Correlation of Directions of Displacement Vectors

In order to make quantitative assessment of spatial correlation of directions of displacement vectors, correlation function of the direction vectors[16] is calculated. Calculated correlation functions are shown in Figure 7 for four normal modes with frequencies 4.1 cm^{-1}(#1), 6.0 cm^{-1}(#3), 11.1 cm^{-1}(#10) and 16.8 cm^{-1}(#17). In all four curves, the function $C_i(d)$ (see equation 18 in reference 16) decreases monotonically from unity to vanish at certain values d_1. As interatomic distance d becomes larger than d_1, $C_i(d)$ becomes negative and then again vanishes at certain values d_2, which are about twice d_1. The correlation functions for two modes, #1 and #2, have similar appearances. In these modes, atom pairs separated by about 40 Å have the positive correlations of about 0.8, and the values of d_1 and d_2 are 13 Å and 29 Å, respectively (Fig. 7a). The correlation functions for modes with mode number equal to or larger than #3 (Fig. 7b–d), indicate that motions of atom pairs separated more are less correlated in these modes. The larger the mode number, the smaller the values of d_1 and d_2. These results are consistent with

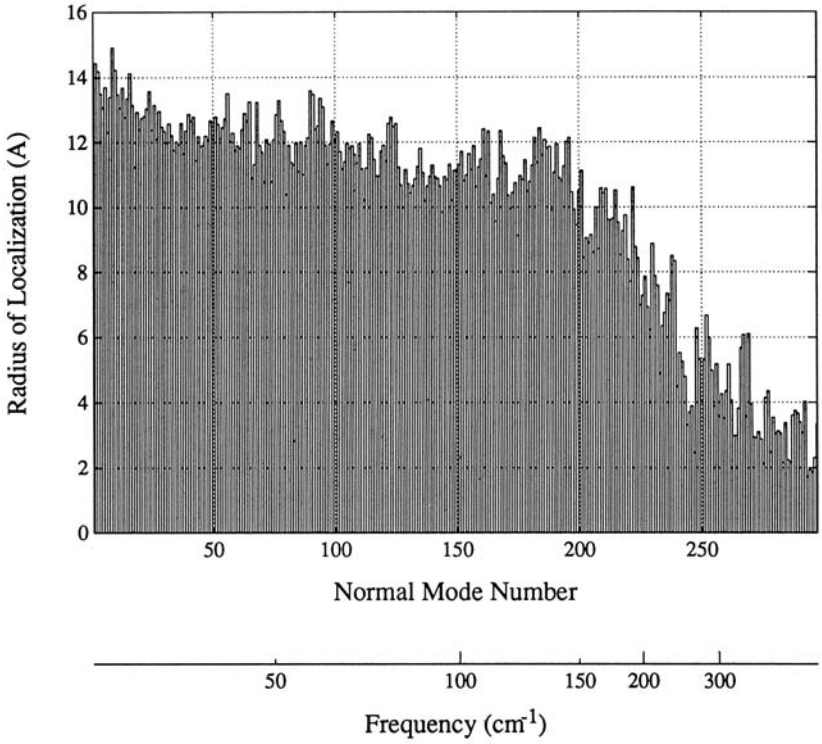

Fig. 5. Radius of localization of normal modes plotted against sequential normal mode number and frequency. The sequential normal mode number is given in the ascending order of frequency.

the results obtained in the section, Localization of Atomic Displacement Vectors in Each Mode, which indicate that motion of atoms in modes with high frequencies are localized in narrower regions.

By regarding each normal mode effectively as a plane wave, and $2d_1$ as its wavelength, we can calculate an effective velocity of each mode. Velocity of a plane wave in a continuous elastic medium is given roughly by $(E/\rho)^{1/2}$, where E and ρ are Young's modulus and the mass density of the medium. By using this expression and calculated velocities of equivalent plane waves and by assuming 1 g cm^{-1} for the value of ρ, effective values of Young's modulus of the protein molecule in the typical normal modes are estimated. The effective values of the Young's modulus for the four lowest frequency modes corresponding to Figure 7 are 0.011×10^{11}, 0.012×10^{11}, 0.035×10^{11}, 0.075×10^{11} dyn·cm^{-2}, respectively. The value for 4.1 cm^{-1} mode is a bit larger than 0.008×10^{11} dyn·cm^{-2} for the mode with the lowest frequency 4.4 cm^{-1} in BPTI. The difference may be related to the fraction of residues involved in β-sheets in the molecule.

Fluctuations of Secondary Structures

There is an antiparallel β-sheet (V19-N32) in mEGF. Motion of this structural element in each mode is divided into internal and external ones as was done previously for BPTI.[16] Their magnitudes in each mode are plotted in Figure 8. In Figure 8 we see that in modes with frequencies higher than 20 cm^{-1}, the thermal fluctuations of the β-sheet in this molecule are determined mainly by internal motions. Internal and external motions of the β-sheet in two normal modes with frequencies 4.1 and 25.0 cm^{-1} are shown in Figures 9 and 10, respectively. Internal motions in these two modes are roughly of the same magnitudes, while external motions are very large in the former mode and very small in the latter mode in comparison with the magnitudes of the internal motions. This means that in very low frequency modes, which have large contributions to the mass-weighted mean-square fluctuations by a quantity proportional to the inverse square of its frequency, the β-sheet structure behaves relatively rigidly and undergoes mostly external motions, thus making a large contribution to the mean-square fluctuations. As the frequency becomes larger, the external motion becomes smaller rapidly.

Very Low Frequency Modes

The site dependence of rms fluctuation of mainchain atoms was found in the section, Fluctuation of C^{α} Atoms, to be determined mainly by modes with frequencies less than 30 cm^{-1}. Of these modes, three with very low frequencies are studied in detail with respect to their dynamic characteristics. Stereo drawings of atomic displacements in

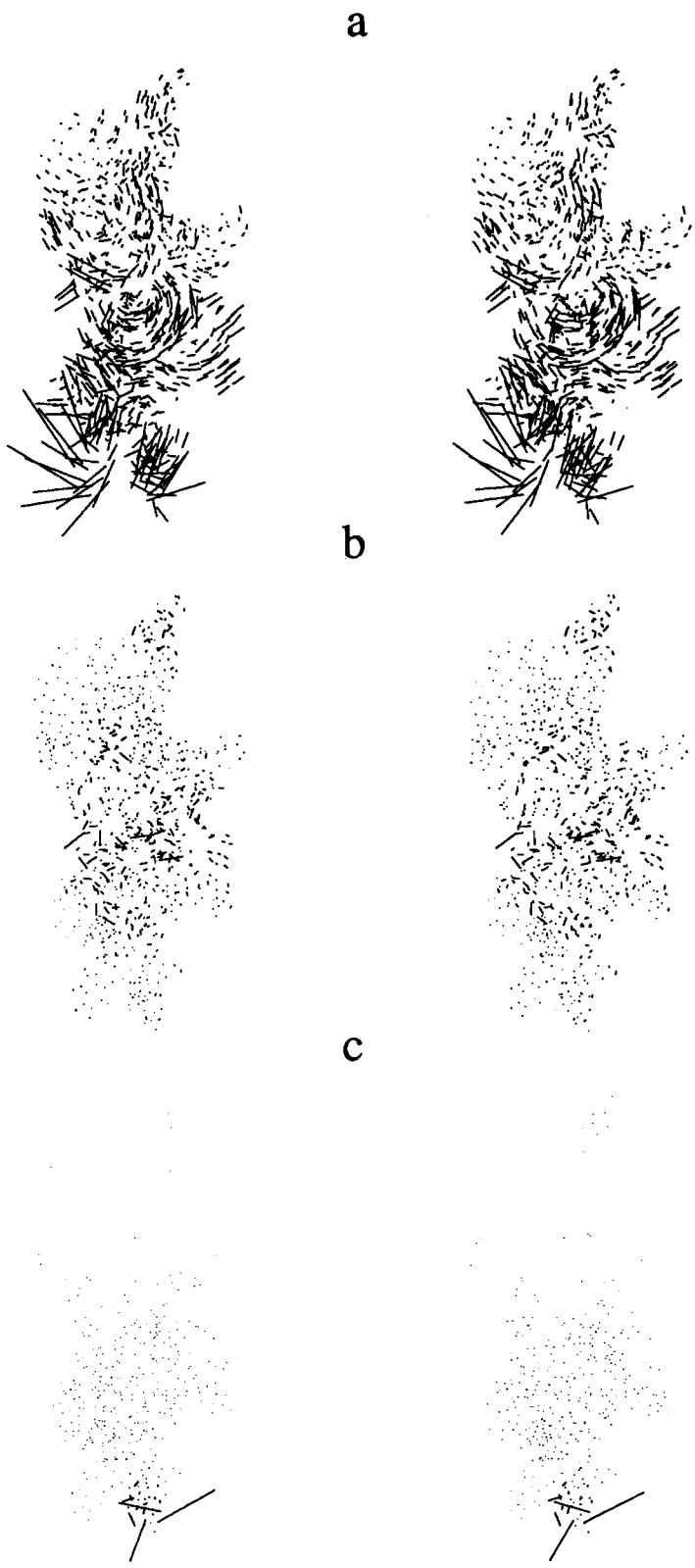

Fig. 6. Stereo drawing of atomic displacement vectors in modes with frequencies 30.8 cm^{-1} **(a)**, 150.7 cm^{-1} **(b)**, and 350 cm^{-1} **(c)**, respectively. The molecule is in the same view as in Figure 1. The magnification factor of these vectors is 50.

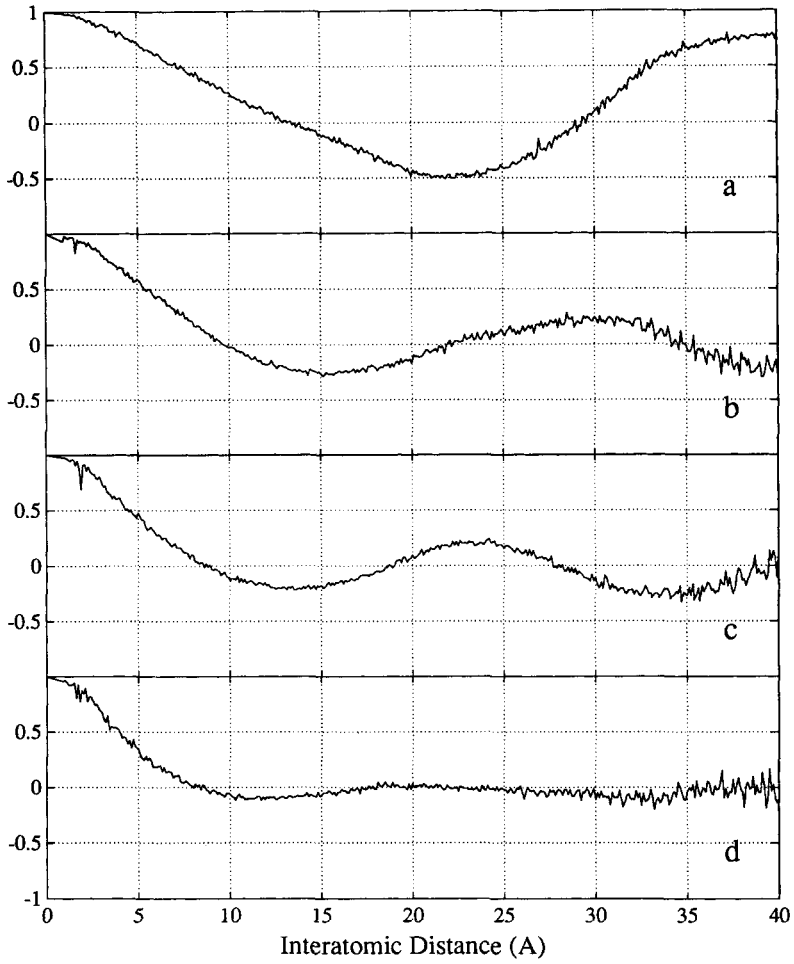

Fig. 7. Correlation function of direction vectors of atomic displacements calculated for four normal modes with frequencies 4.1 cm^{-1} **(a)**, 6.0 cm^{-1} **(b)**, 11.1 cm^{-1} **(c)**, and 16.8 cm^{-1} **(d)**.

these modes are shown in Figure 11. In order to study relative movements between residues, maps for distance fluctuations between residues are also prepared and are given in Figure 12 for the three modes. From patterns of symbols in the triangular maps, we can identify rigid and flexible segments along the chain. A rigid segment along the chain appears as a white triangle on the diagonal. A region near the diagonal corresponding to a flexible segment is filled with symbols. We can also see relative displacements between these segments from the map.

By examination of Figures 11 and 12 for the three modes, we see the following.

Mode with frequency of 4.1 cm^{-1}

This mode corresponds to the hinge-bending motion between the two domains of mEGF. In this motion, the N-terminal domain (N1-N32) is almost rigid. However, the C-terminal domain is found to consist of three rigid segments. Two segments, C33-D46 and G51-R53, are observed moving in the same directions, but L47-W50 moves in the opposite direction.

Mode with frequency of 5.2 cm^{-1}

In this motion, the C-terminal domain (C33-R53) is almost rigid. The N-terminal domain is found to consist of three rigid segments, N1-S8, S9-G18, and V19-C31. Two segments, S9-G18 and C31-R53, are observed moving in the same direction, but V19-T30 moves in the opposite direction. N1-S8 is observed moving in the direction independent of other segments. V19-T30 is located in the β-sheet. In this mode, the thermal fluctuation of the β-sheet is mainly determined by an external motion (Fig. 8).

Mode with frequency of 6.0 cm^{-1}

This mode is a rather complex oscillation involving both twisting and bending. In this motion, two segments, S18-S25 and G27-I35, have small dis-

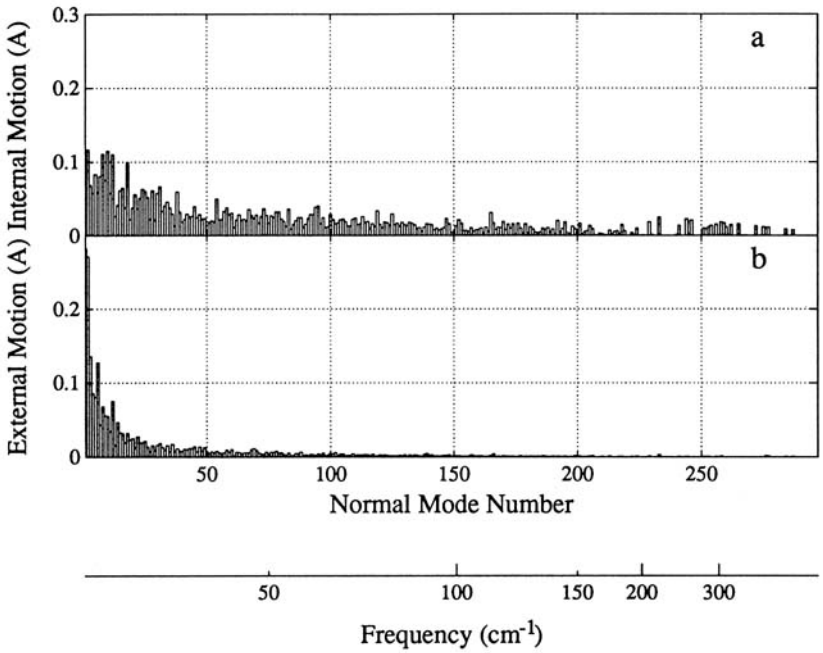

Fig. 8. Magnitudes of internal **(a)** and external **(b)** motions of the β-sheet in each normal mode plotted against the serial normal mode number and frequency.

tance fluctuations. These segments correspond to β-strands which belong to the β-sheet.

DISCUSSION

Kohda et al.[8] proposed a mitten model of mEGF. This model not only describes the rough shape of the static structure, but also suggests the existence of a motion corresponding to the opening and closing of the two domains, the palm and the thumb. It is further implicated that this motion is functionally important, i.e., is involved in the process of binding to the receptor. This type of motion, hinge-bending motion, has also been assumed to exist and to be functionally important in lysozyme. In the case of lysozyme, the normal mode with the lowest frequency has been shown to correspond very faithfully to the hinge-bending motion.[17] Therefore, it is a natural idea to carry out the normal mode analysis for mEGF, and to see if the hinge-bending motion exists also in mEGF. The result has indeed confirmed this expectation. The mode with the lowest frequency, 4.1 cm^{-1}, corresponds to the hinge-bending motion between the two domains. In this motion, each domain is observed moving in the direction suggested by the mitten model, though the C-terminal domain becomes slightly deformed during the motion. Even though the existence of the hinge-bending motion is confirmed, we cannot at the moment directly verify its involvement in the process of binding to the receptor.

We compare the results of the normal mode analysis of mEGF with those of BPTI and human lysozyme.

Distribution of the Calculated Frequencies

The frequencies of each of the three molecules are distributed to the value from about 4 cm^{-1} to about 950 cm^{-1}. The fraction of the modes of BPTI with frequencies below 200 cm^{-1} are 7% larger than that of mEGF.

Fluctuations of Dihedral Angles

The average values of rms fluctuations for the dihedral angles, ω, ϕ and ψ, of each of the three molecules are about 5°, 8° and 8°, respectively. The values of BPTI are a bit larger than those of the others. The largest peak frequency of backbone dihedral angles of BPTI are observed to be a little smaller than that of mEGF. It suggests that BPTI behaves slightly softer than mEGF. The same tendency is observed also in the effective Young's modulus for the mode with the lowest frequency.

Fluctuations of Atom Positions

Both in BPTI and mEGF, modes with frequencies less than 30 cm^{-1} essentially determine the site dependence of the thermal fluctuations. Also in human lysozyme, ten lowest frequency modes have been shown essentially to determine the site dependence.

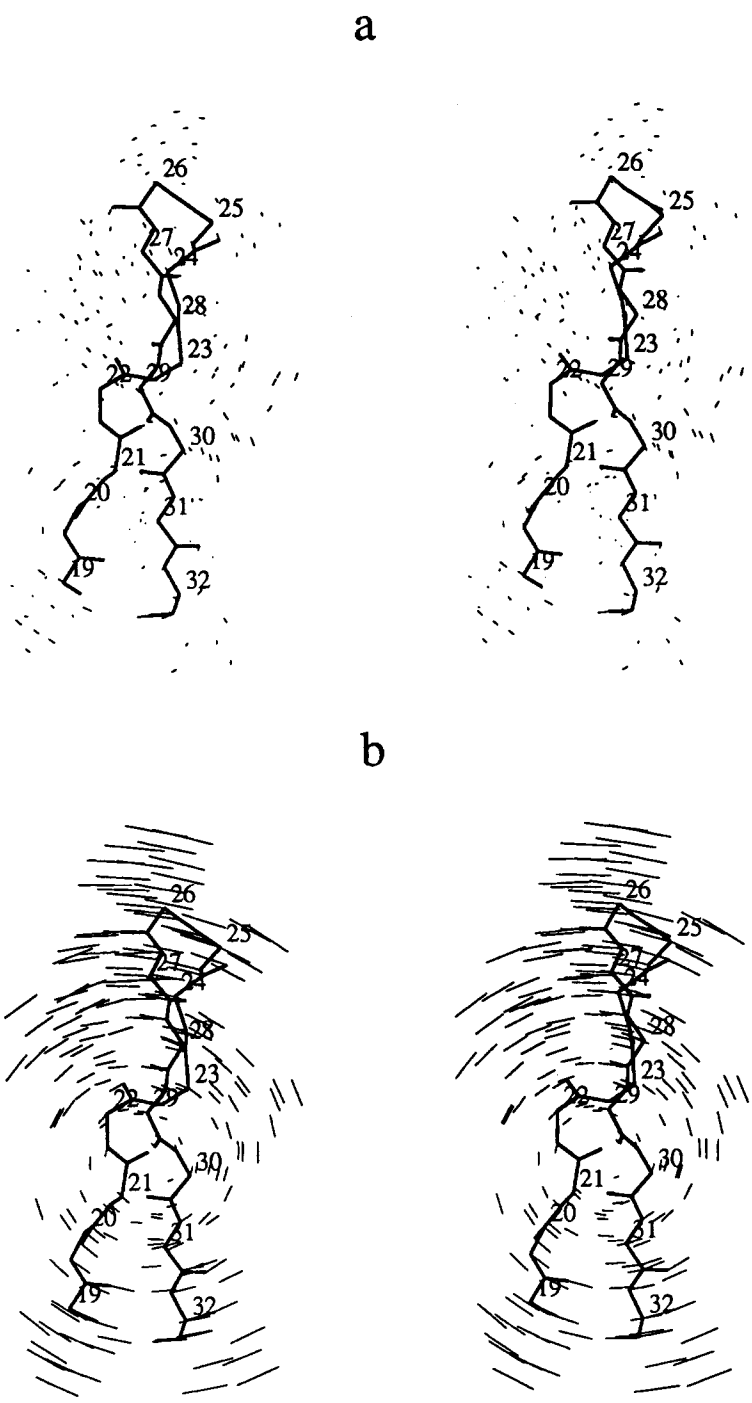

Fig. 9. Stereo drawings of internal **(a)** and external **(b)** motions of the β-sheet in the normal mode with frequency 4.1 cm^{-1}. The magnification factor of these vectors is 5.

Localization of Atomic Displacement Vectors

The radius of localization of normal modes of mEGF plotted against frequency has very similar shape to that of BPTI, except that the values of the radii are a little larger in mEGF than in BPTI.

Very Low Frequency Modes

The motion due to modes with very low frequencies of mEGF is entirely different from that of BPTI. In the modes with frequencies 4.1 and 5.2 cm^{-1} of mEGF, atom pairs separated by about 40 Å have the

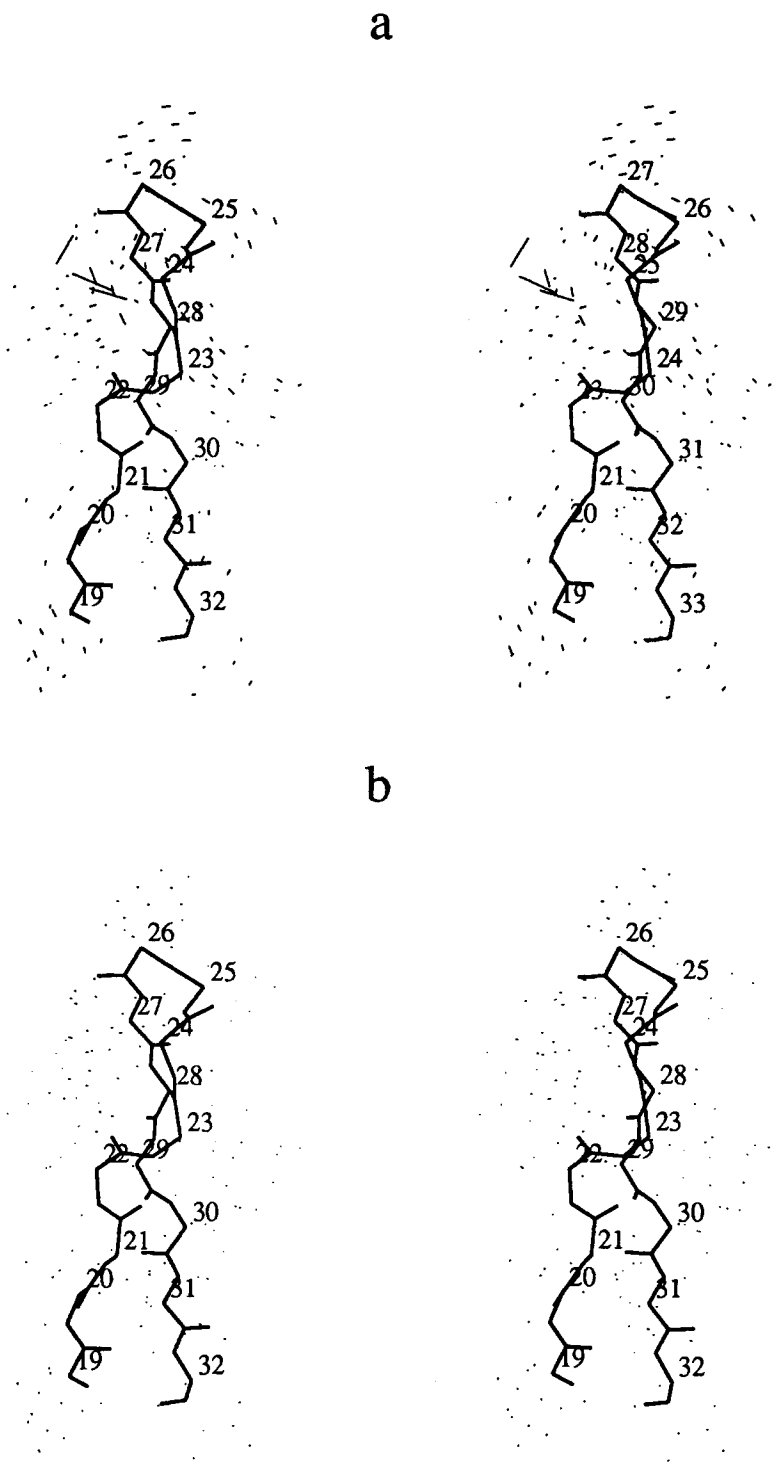

Fig. 10. Stereo drawings of internal **(a)** and external **(b)** motions of the β-sheet in the normal mode with frequency 25.0 cm^{-1}. The magnification factor of these vectors is 5.

positive large correlations. However, such correlations are not observed in any modes of BPTI. The correlation functions for modes with frequencies 4.4–30 cm^{-1} of BPTI have similar appearance with those for modes with frequencies 6.0–11.1 cm^{-1} of mEGF. The lowest frequency modes of both mEGF and human lysozyme are characterized as "hinge-bending" motions. The third lowest modes of both

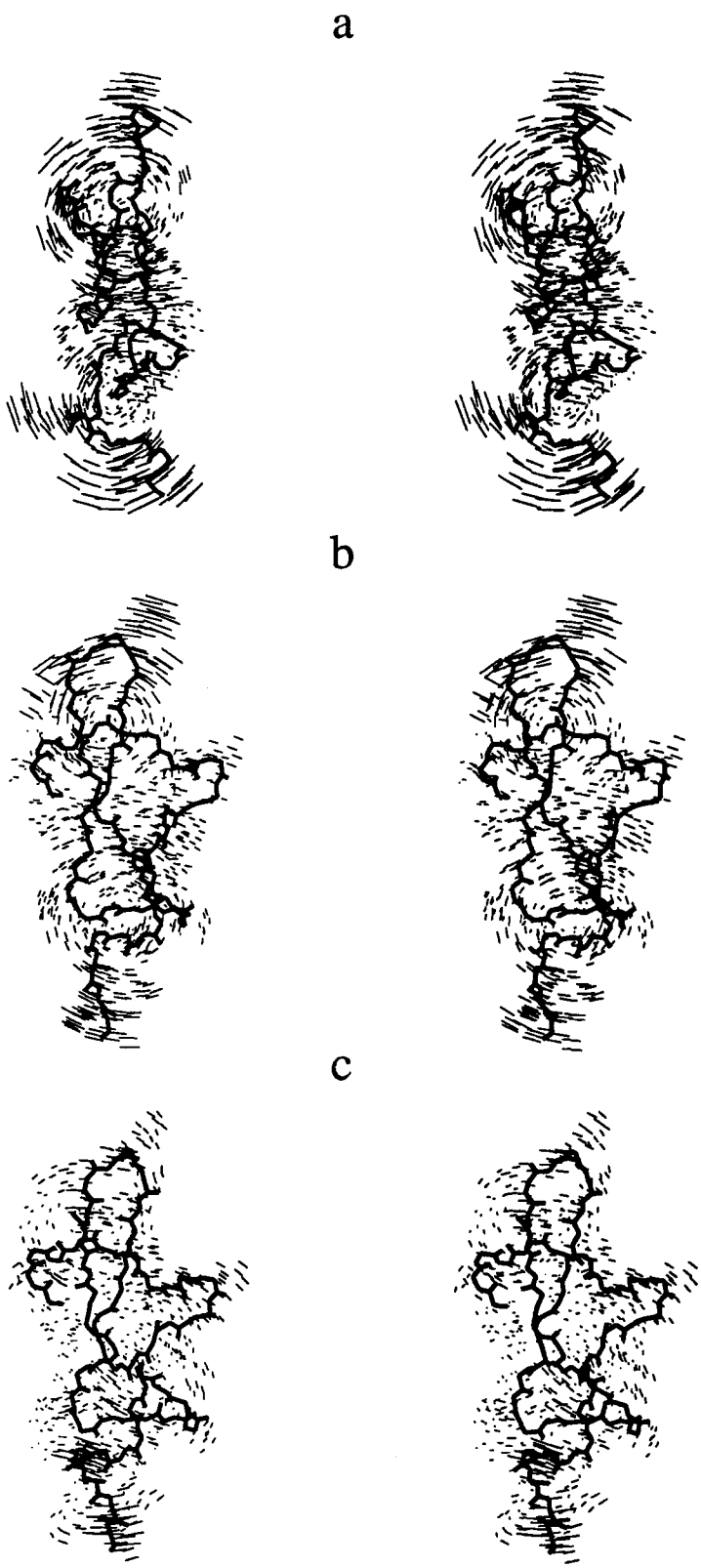

Fig. 11. Stereo drawings of atomic displacements in three lowest frequency modes with frequencies 4.1 cm^{-1} **(a)**, 5.2 cm^{-1} **(b)**, and 6.0 cm^{-1} **(c)**. The displacement vectors are magnified by a factor 10.

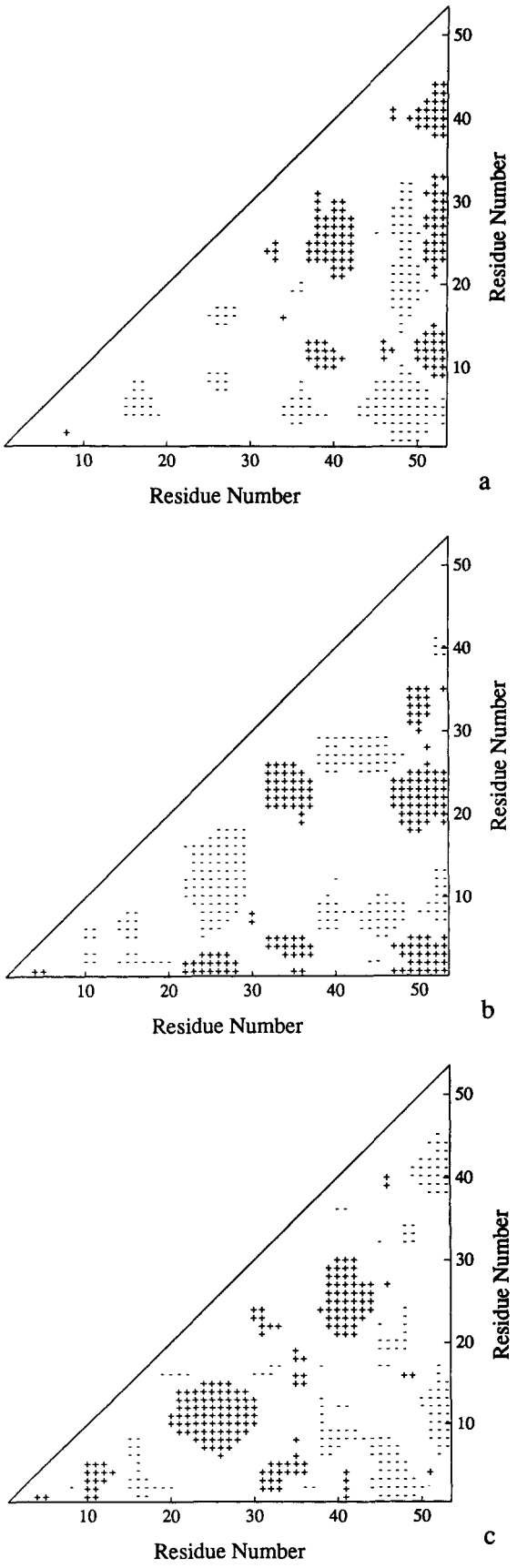

Fig. 12. Triangular maps showing the change of distances between two residues due to three lowest frequency modes with frequencies 4.1 cm^{-1} **(a)**, 5.2 cm^{-1} **(b)**, and 6.0 cm^{-1} **(c)**. The change of distance between two residues is calculated as the average change between the main chain (N, C^{α}, C′, O) atoms of the two residues. This quantity is normalized by dividing by the average change of all the possible distances in the molecule. A blank means that the absolute value of this quantity is less than unity. The absolute value for a pair of residues with either + or − is equal to or larger than unity. A phase of distance fluctuation with the mark + is opposite to one with the mark −.

mEGF and BPTI correspond to rather complex oscillations involving both twisting and bending.

The results of comparison summarized above suggest that the fluctuations given as a sum of contributions from all modes have similar character mostly independent of size and kind of the molecule, and that individual normal modes with very low frequencies are good indexes to characterize the dynamics of each molecule.

ACKNOWLEDGMENTS

This work has been supported by grants from Ministry of Education, Science and Culture, Japan, and from International Human Frontier Science Program Organization. Computations have been carried out at the commuting centers at Kyoto University and at Institute for Molecular Science.

REFERENCES

1. Cohen, S. Isolation of a mouse submaxillary gland protein accelerating incisor eruption and eyelid opening in the new born animal. J. Biol. Chem. 237:1555–1562, 1962.
2. Savage, C.R., Jr., Inagami, T., Cohen, S. The primary structure of epidermal growth factor. J. Biol. Chem. 247: 7612–7621, 1972.
3. Savage, C.R., Jr., Hash, J.H., Cohen, S. Epidermal growth factor location of disulfide bonds. J. Biol. Chem. 248:7669–7672, 1973.
4. Sporn, M.B., Roberts, A.B. Autocrine growth factors and cancer. Nature (London) 313:745–747, 1985.
5. Sporn, M.B., Todaro, G.J. Autocrine secretion and malignant transformation of cells. N. Eng. J. Med. 303:878–880, 1980.
6. Buckley, A., Davidson, J.M., Kamerath, C.D., Wolt, T.B., Woodward, S.C. Sustained release of epidermal growth factor accelerates wound repair. Proc. Natl. Acad. Sci. USA 82:7340–7344, 1985.
7. Kohda, D., Inagaki, F. Complete sequence-specific ^1H nuclear magnetic resonance assignments for mouse epidermal growth factor. J. Biochem. 103:554–571, 1988.
8. Kohda, D., Gō, N., Hayashi, K., Inagaki, F. Tertiary structure of mouse epidermal growth factor determined by two-dimensional ^1H NMR. J. Biochem. 103:741–743, 1988.
9. Montelione, G.T., Wüthrich, K., Nice, E.C., Burgess, A.W., Scheraga, H.A. Identification of two anti-parallel β-sheet conformations in the solution structure of murine epidermal growth factor by proton magnetic resonance. Proc. Natl. Acad. Sci. USA 83:8594–8598, 1986.
10. Montelione, G.T., Wüthrich, K., Nice, E.C., Burgess, A.W., Scheraga, H.A. Solution structure of murine epidermal growth factor: Determination of the polypeptide backbone chain-fold by nuclear magnetic resonance and distance geometry. Proc. Natl. Acad. Sci. USA 84:5226–5230, 1987.
11. Montelione, G.T., Wüthrich, K., Scheraga, H.A. Sequence-specific ^1H NMR assignments and identification of slowly exchanging amid protons in murine epidermal growth factor. Biochemistry 27:2235–2243, 1988.
12. Montelione, G.T., Wüthrich, K., Burgess, A.W., Nice, E.C., Wagner, G., Gibson, K.D., Scheraga, H.A. Solution struc-

ture of murine epidermal growth factor determined by NMR spectroscopy and refined by energy minimization with restraints. Biochemistry 31:236–249, 1992.
13. Katsuura, M., Tanaka, S. Topographic analysis of human epidermal growth factor by monospecific antibodies and synthetic peptides. J. Biochem. 106:87–92, 1989.
14. Campion, A.R., Matsunami, R.K., Engler, D.A., Niyogi, A.K. Biochemical properties of site-directed mutants of human epidermal growth factor: Importance of solvent-exposed hydrophobic residues of the amino-terminal domain in receptor binding. Biochemistry 29:9988–9993, 1990.
15. Burgess, A.W., Lloyd, C.J., Smith, S., Stanley, E., Walker, F., Fabri, L., Simpson, R.J., Nice, E.C. Murine epidermal growth factor: Structure and function. Biochemistry 27: 4977–4985, 1988.
16. Nishikawa, T., Gō, N. Normal mode of vibration in bovine pancreatic trypsin inhibitor and its mechanical property. Proteins 2:308–329, 1987.
17. Gibrat, J.-F., Gō, N. Normal mode analysis of human lysozyme: Study of the relative motion of two domains and characterization of the harmonic motion. Proteins 8:258–279, 1990.
18. Braun, W., Gō, N. Calculation of protein conformations by proton-proton distance constraints: A new efficient algorithm. J. Mol. Biol. 186:611–626, 1985.
19. Endo, S., Wako, H., Nagayama, K., Gō, N. A new version of DADAS (distance analysis in dihedral angle space) and its performance. Nato ASI Series A225:233–251, 1991.
20. Némethy, G., Pottle, M.S., Scheraga, H.A. Energy parameters in polypeptides. 9. Updating of geometrical parameters, nonbonded interactions, and hydrogen bond interactions for the naturally occurring amino acids. J. Phys. Chem. 87:1883–1887, 1983.